



 Cite this: *RSC Adv.*, 2021, 11, 9865

# A one-pot synthesis of AgBr/Ag<sub>3</sub>PO<sub>4</sub> composite photocatalysts†

 Jiahang Su,<sup>a</sup> Yitao Fan,<sup>a</sup> Yu Yan,<sup>b</sup> Tao Liu,<sup>a</sup> Hongshuang Li,<sup>a</sup> Zhenyu Li <sup>\*a</sup> and Fujiao Song<sup>\*c</sup>

In this study, an AgBr/Ag<sub>3</sub>PO<sub>4</sub> (ABAP) photocatalyst has been prepared *via* a facile one-pot anion-exchange method. SEM, XRD, XPS and UV-Vis DRS characterization techniques are carried out to study the structural and physicochemical characteristics of the AgBr/Ag<sub>3</sub>PO<sub>4</sub> composites. The ABAP photocatalyst exhibited outstanding photocatalytic capability for the photodegradation of rhodamine B (RhB) under visible light irradiation. The optimal ABAP-48% composite displayed the highest photocatalytic activity; a complete degradation was attained in 25 min under visible light irradiation. The excellent stability and reusability of ABAP catalysts were examined by five subsequent runs. A probable degradation mechanism of ABAP composites was carefully surveyed. Furthermore, radical trapping experiments confirmed that the <sup>•</sup>O<sub>2</sub><sup>-</sup> radical was the main active species in the photodegradation reaction.

 Received 5th December 2020  
 Accepted 4th February 2021

DOI: 10.1039/d0ra10265b

[rsc.li/rsc-advances](http://rsc.li/rsc-advances)

## 1. Introduction

With the rapid development of the textile and paper industries, a great amount of effluent-containing numerous organic dyes has triggered water pollution issues, which has attracted considerable attention of scientists.<sup>1</sup> The textile effluent consists of suspended solids, grease, lint, surfactants and numerous organic pollutants.<sup>2</sup> In order to prevent textile waste water from polluting the environment, researchers began to look for ways to treat textile waste water. However, researchers have found that traditional treatment methods, such as physical, chemical and biological methods, could not completely remove complex mixtures and non-biodegradable pollutants from the water.<sup>3</sup> The semiconductor-based photocatalytic technique has tremendously engaged numerous scholars' attention for purifying air and water due to its advantages of being environmentally friendly and inexpensive.<sup>4</sup>

However, the photocatalytic efficiency of pure Ag<sub>3</sub>PO<sub>4</sub> is limited by the high recombination rate of its photo-induced electron-hole pairs and poor stability in the photocatalytic process.<sup>5</sup> So far, numerous strategies have been explored to solve the above-mentioned problems, such as metal doping, construction of semiconductor heterojunctions and carbon-

based material recombination. Among these reports, the construction of Ag<sub>3</sub>PO<sub>4</sub>-based heterostructure photocatalysts with other semiconductors is an efficient way to effectively adjust the bandgap structure, and discourage the reorganization of photogenerated electron-hole pairs.<sup>6</sup> Until now, there are numerous reports about Ag<sub>3</sub>PO<sub>4</sub>-based heterostructure photocatalysts, including M/Ag<sub>3</sub>PO<sub>4</sub> (M = Pt, Pd, and Au),<sup>7</sup> Ag@Ag<sub>3</sub>PO<sub>4</sub>@ZnO,<sup>8</sup> Ag<sub>2</sub>MoO<sub>4</sub>/Ag<sub>3</sub>PO<sub>4</sub>,<sup>9</sup> Ag<sub>2</sub>S/Ag<sub>3</sub>PO<sub>4</sub>,<sup>10</sup> Ag/Ag<sub>3</sub>PO<sub>4</sub>/WO<sub>3</sub>,<sup>11</sup> g-C<sub>3</sub>N<sub>4</sub>/Ag<sub>3</sub>PO<sub>4</sub>,<sup>12</sup> GO/Ag<sub>3</sub>PO<sub>4</sub>/AgBr,<sup>13</sup> and nitrogen-doped carbon quantum dots/Ag<sub>3</sub>PO<sub>4</sub>.<sup>14</sup> Among various Ag-based materials, AgBr is particularly attractive owing to its facile synthesis route, appropriate band gap (~2.6 eV) as well as excellent photocatalytic activity.<sup>15</sup> AgBr is regarded as a feasible photocatalyst as it can be excited to generate electron-hole pairs under visible light irradiation. Thus, the weak stability of pure AgBr is a drawback in practical photocatalytic applications. In recent years, numerous AgBr-based heterostructure photocatalysts, such as AgBr/Bi<sub>2</sub>WO<sub>6</sub>,<sup>16</sup> AgBr/Ag<sub>3</sub>PO<sub>4</sub>,<sup>17</sup> AgBr/ZnO,<sup>18</sup> AgBr/MgBi<sub>2</sub>O<sub>6</sub>,<sup>19</sup> Ag<sub>2</sub>MoO<sub>4</sub>/Ag/AgBr<sup>20</sup> and g-C<sub>3</sub>N<sub>4</sub>/GO/AgBr,<sup>21</sup> have been successfully synthesized due to their strong visible light response, high photocatalytic performance, and ability to inhibit electron holes induced by composite light, effectively alleviating the problem of photocorrosion. Among these composite photocatalysts, although AgBr/Ag<sub>3</sub>PO<sub>4</sub> composite photocatalysts have also been extensively studied, previous studies have reported that the two-step method to synthesize AgBr/Ag<sub>3</sub>PO<sub>4</sub> photocatalysts has some disadvantages, such as complicated synthesis process, poor photocatalytic activity and low stability of the products.<sup>22,23</sup> A few studies related to the decoration of AgBr NPs onto the surface of Ag<sub>3</sub>PO<sub>4</sub> by one-pot method have also been reported. However, the preparation of efficient and environmentally friendly AgBr/Ag<sub>3</sub>PO<sub>4</sub>

<sup>a</sup>School of Chemical Engineering, Changchun University of Technology, Changchun 130012, P. R. China. E-mail: cclzy2001@163.com

<sup>b</sup>Municipal Engineering Northeast Design and Research Institute Co. Ltd, Changchun 130112, P. R. China

<sup>c</sup>School of Environmental Science and Engineering, Yancheng Institute of Technology, Yancheng, 224051, P. R. China. E-mail: song\_fj2006@126.com

† Electronic supplementary information (ESI) available: Scanning electron microscope images of the pure AgBr nanoparticles, XPS of the survey spectrum of ABAP-48% composites, with a brief description. See DOI: 10.1039/d0ra10265b



photocatalysts with uniformly distributed AgBr NPs on the surface of  $\text{Ag}_3\text{PO}_4$  is crucial to achieve ideal results.

The aim of this project is to prepare a series of ABAP photocatalysts *via* a one-pot anion-exchange method. The performance of the absorption of ABAP photocatalysis with different contents of Br/P was evaluated by the comparing removal rates of RhB. The optical photo-degradation of the ABAP composite in the visible-light range can be highly increased owing to efficient photogenerated electron and hole separation and shifting mechanism. In addition, the possible photodegradation mechanism of the ABAP photocatalyst is also proposed.

## 2. Experiment

### 2.1 Materials and synthesis

Silver nitrate ( $\text{AgNO}_3$ ), sodium bromide ( $\text{NaBr}$ ) and absolute ethanol were purchased from Beijing Chemical Works. Sodium phosphate monobasic dihydrate ( $\text{NaH}_2\text{PO}_4$ ), hexamethylene tetramine (HMT), isopropanol (IPA), ammonium oxalate (AO) and *p*-benzoquinone (BQ) were purchased from Sinopharm Chemical Reagent Co., Ltd. All of the reagents used in this experiment were of analytical reagent grade without further purification. Ultrapure water utilized in the experiments was obtained from a Milli-Q ultrapure (18.25 M $\Omega$  cm) system.

The AgBr/ $\text{Ag}_3\text{PO}_4$  composites were synthesized *via* a facile one pot *in situ* anion-exchange method at room temperature. In a typical synthesis, 0.315 g HMT was added to 40 ml of 0.05 M  $\text{AgNO}_3$  solution under vigorous stirring, and then, the solution became milky white. The mixture was continually stirred for 15 min at room temperature. Subsequently,  $\text{NaH}_2\text{PO}_4$  (0.15 M) was added dropwise to the above solution, and continuously stirred for another 15 min. Afterwards, an NaBr (0.1 M) solution with different volume was added drop by drop to the above solution, and stirred for another 4 h. Finally, the precipitates obtained by centrifugation were then washed several times with ultrapure water and absolute alcohol, dried in an oven at 80 °C for 24 h. The products were named as ABAP-*X*% (*X* is the theoretical molar ratio of Br to P in AgBr/ $\text{Ag}_3\text{PO}_4$  composites). As a reference, pure AgBr or  $\text{Ag}_3\text{PO}_4$  were synthesized *via* the same method without the addition of  $\text{NaH}_2\text{PO}_4$  or NaBr.

### 2.2 Characterization

The morphology and microstructure of the samples were characterized by scanning electron microscopy (SEM) using a model XL30ESEM FEG. The crystalline structure and phase purity of the samples were confirmed *via* X-ray diffraction (XRD) on a Rigaku/Smartlab instrument with the X-ray diffractometer with Cu K $\alpha$  radiation at a scan rate of 0.01° 2 $\theta$  s<sup>-1</sup>. UV-Vis diffuse reflectance spectra (UV-Vis DRS) were recorded on an Agilent/Cary 5000 using BaSO<sub>4</sub> as the reference material.

### 2.3 Photocatalytic activity test

RhB was utilized as the simulated dye wastewater to assess the photocatalytic activity of the as-prepared samples. Visible light irradiation was provided by a 500 W xenon lamp (Shanghai Jia Peng Technology Co., Ltd.) equipped with a glass filter ( $\lambda > 420$  nm),

which was positioned about 7–10 cm above the solution. In this experiment, the samples were added into a cylindrical quartz glass reactor with 50 ml RhB solution. Before light irradiation, the suspension was stirred for 30 min in dark to ensure the adsorption-desorption equilibrium between the catalysts and RhB solution. In the experimental process, 5 ml of the suspension was taken out at the intervals of the same duration, and immediately separated by centrifugation. Subsequently, the supernatant was monitored using a TU-1901 dual-beam UV-Vis spectrophotometer (Beijing Purkinje General Instrument Co., Ltd.) at the characteristic absorption wavelength ( $\lambda_{\text{max}} = 554$  nm) of RhB. The photocatalytic degradation rate could be estimated according to the following eqn (1):

$$\eta = \frac{C_0 - C_t}{C_0} \times 100\% = \frac{A_0 - A_t}{A_0} \times 100\% \quad (1)$$

where  $C_0$ ,  $A_0$  and  $C_t$ ,  $A_t$  are the initial concentration and ultimate concentration of RhB during the photocatalytic reaction, respectively. The active species trapping experiments of ABAP-*X*% composites were carried out under visible light irradiation for RhB degradation with the addition of isopropanol (IPA), ammonium oxalate (AO) and *p*-benzoquinone (BQ) as scavengers for  $\cdot\text{OH}$ ,  $\text{h}^+$  and  $\cdot\text{O}_2^-$ .

## 3. Results and discussion

### 3.1 Sample characterization

XRD was used to validate the crystalline structure of the as-synthesized samples. It can be seen from Fig. 1 that all of the identified peaks in the XRD pattern could be attributed to the body-centered cubic phase  $\text{Ag}_3\text{PO}_4$  (JCPDS no. 06-0505), indicating that  $\text{Ag}_3\text{PO}_4$  had a body-centered cubic structure. The strong and sharp peaks of  $\text{Ag}_3\text{PO}_4$  nanoparticles indicated its high crystallinity. Close to the JCPDS cards of pristine AgBr (no. 06-0438) (Fig. 1(g)), the characteristic diffraction peaks belong to the face-centered cubic structure. No impurity peaks were detected in the sample, which showed that the samples were pure AgBr phase. Compared to pure  $\text{Ag}_3\text{PO}_4$  and AgBr, the peak intensities of ABAP composites were obviously weaker. It seemed that a part of the XRD signal of  $\text{Ag}_3\text{PO}_4$  particles was

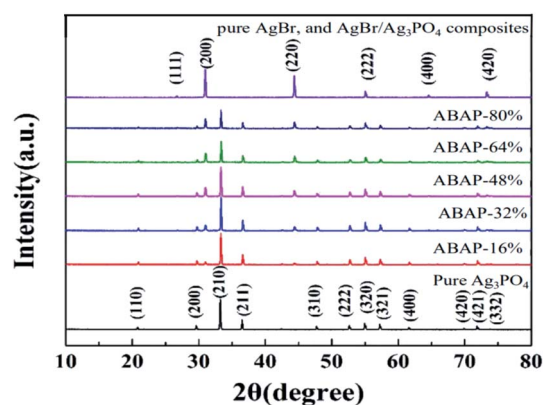


Fig. 1 X-ray diffraction patterns of (a) pure  $\text{Ag}_3\text{PO}_4$ , (b) ABAP-16%, (c) ABAP-32%, (d) ABAP-48%, (e) ABAP-64%, (f) ABAP-80%, (g) pure AgBr, and AgBr/ $\text{Ag}_3\text{PO}_4$  composites.

hindered by the surface-coated AgBr, which contributed to the decrease in the intensity of XRD diffraction peaks. It is expected that the XRD pattern of the ABAP composites clearly matched with the polycrystalline structures of AgBr and  $\text{Ag}_3\text{PO}_4$ , suggesting that AgBr and  $\text{Ag}_3\text{PO}_4$  maintained pure phase, and there were no impurities in the ABAP composites. It is indicated that the ABAP composites have been successfully prepared.

The comparative morphology of the as-synthesized  $\text{Ag}_3\text{PO}_4$  and ABAP composites with different concentrations of Br/P were characterized by SEM images shown in Fig. 2. It can be observed that the polyhedral structure particle is the  $\text{Ag}_3\text{PO}_4$  material in Fig. 2(a) (blue circle), and the average diameter of  $\text{Ag}_3\text{PO}_4$  is 1  $\mu\text{m}$ . Furthermore, we can clearly observe that the surface of  $\text{Ag}_3\text{PO}_4$  is very smooth and clean. The pure AgBr nanoparticles are irregular aggregates composed of grains with diameters of 2 to 7 nm (Fig. S1<sup>†</sup>). It can be seen in Fig. 2(b) that there are a few cluster

particles coated on the smooth surface of  $\text{Ag}_3\text{PO}_4$  (red circle), which are irregularly aggregated AgBr nanoparticles. After coating with an AgBr layer, we can obviously see that AgBr nanoparticles were attached closely to the surface of  $\text{Ag}_3\text{PO}_4$ , which is favourable to the building of heterojunction with different concentrations of Br/P between  $\text{Ag}_3\text{PO}_4$  and AgBr (Fig. 2(c)–(f)). From the SEM images, we can see that ABAP composites have nearly the same morphology as that of  $\text{Ag}_3\text{PO}_4$ . During the one-pot preparation of ABAP-48%,  $\text{Ag}_3\text{PO}_4$  crystals were first synthesized. Then, AgBr was assembled over the outer layer of  $\text{Ag}_3\text{PO}_4$ . This result is in good agreement with the XRD observations discussed above.

The elemental composition and chemical valance state of the notable ABAP-48% were investigated by XPS, and the XPS results are illustrated in Fig. 3. The survey spectrum of ABAP-48% can clearly illustrate the presence of Ag, P, O, and Br in Fig. S2,<sup>†</sup> which originated from  $\text{Ag}_3\text{PO}_4$  and AgBr.<sup>24–26</sup> The

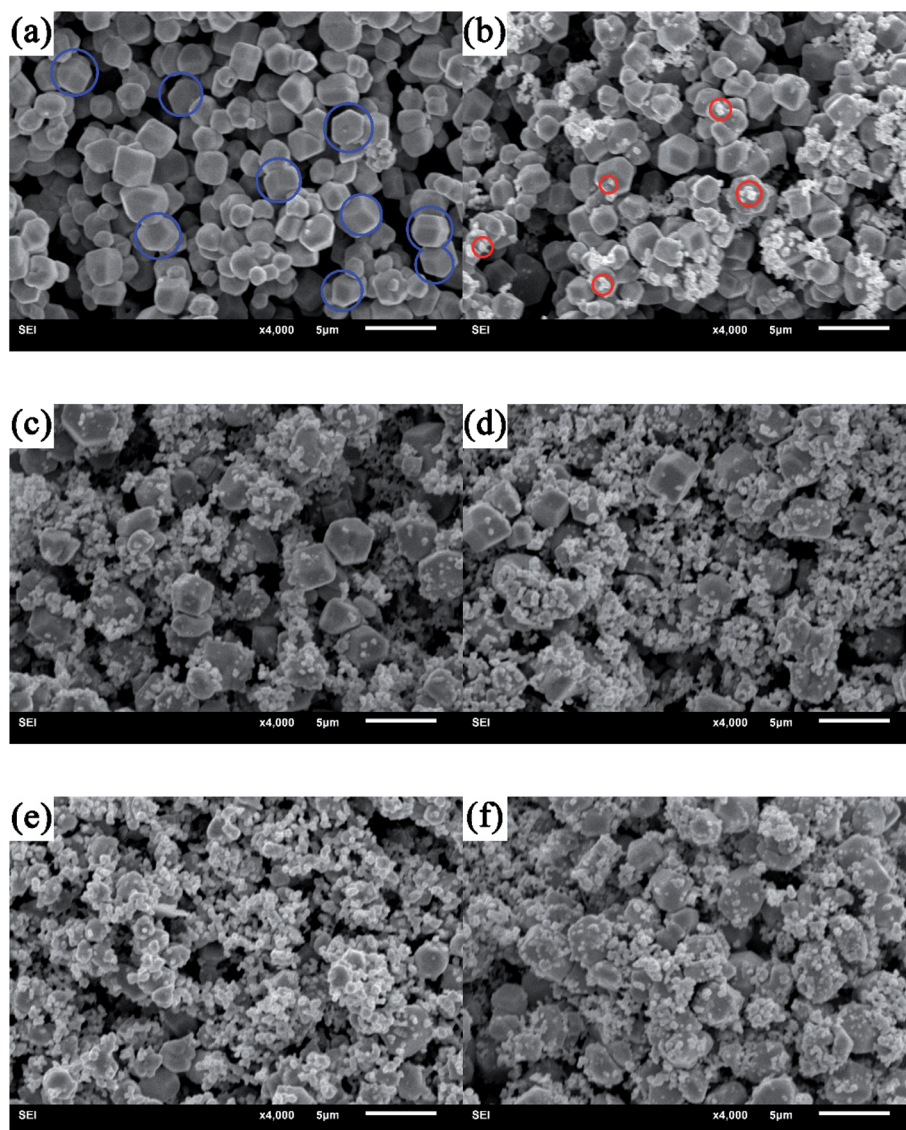


Fig. 2 Typical SEM images of (a) pure  $\text{Ag}_3\text{PO}_4$ , and AgBr/ $\text{Ag}_3\text{PO}_4$  composites, (b) ABAP-16%, (c) ABAP-32%, (d) ABAP-48%, (e) ABAP-64%, (f) ABAP-80%.

noticeable peaks are at 373.8 eV and 367.9 eV of Ag 3d in Fig. 3(a), which correspond to Ag 3d<sub>3/2</sub> and Ag 3d<sub>5/2</sub>, indicating the presence Ag<sup>+</sup> in Ag<sub>3</sub>PO<sub>4</sub> or AgBr. The high-resolution spectrum of Br 3d in Fig. 3(b) demonstrates two peaks at 69.5 and 68.3 eV, which correspond to the binding energies of Br 3d<sub>3/2</sub> and Br 3d<sub>5/2</sub>.<sup>27</sup> The peak located at 132.95 eV in the P 2p spectrum in Fig. 4(c) elucidates the presence of P<sup>5+</sup> in PO<sub>4</sub><sup>3-</sup>. The strong peak in the O 1s spectrum of the sample in Fig. 3(d) at 530.6 eV is ascribed to the oxygen in the Ag<sub>3</sub>PO<sub>4</sub> crystal lattice, and the weak peak at 532.4 eV is due to the chemisorbed H<sub>2</sub>O or OH<sup>-</sup> on the surface of the samples.<sup>28–30</sup> On the basis of the above-mentioned results, the AgBr nanoparticles were successfully attached to the Ag<sub>3</sub>PO<sub>4</sub> surface, in accordance with the XRD and SEM results.

In order to study the light absorption characteristics of the heterojunction composite photocatalytic materials, the UV-Visible diffuse reflection absorption curves of the samples were compared. It can be seen from Fig. 4(a) that Ag<sub>3</sub>PO<sub>4</sub> shows a strong visible light absorption edge located at 550 nm, which is similar to the previous reports.<sup>31,32</sup> The visible light absorption intensity of ABAP-48% is significantly higher than that of pure AgBr and pure Ag<sub>3</sub>PO<sub>4</sub>. The absorption edges of ABAP-48% composite photocatalyst reflect an obvious redshift to 590 nm compared to that of Ag<sub>3</sub>PO<sub>4</sub> and AgBr. This obvious redshift of the absorption edge of the as-prepared sample is ascribed to the excellent sensitization effect of AgBr, which affirms that a large number of photo-induced carriers could be excited by more visible light. This result suggests that Ag<sub>3</sub>PO<sub>4</sub> and AgBr have been composited successfully. Simultaneously, the results also show that the composite photocatalyst has a stronger absorption capacity for visible light, which means the

increase in the efficient response to sunlight, and which is advantageous for the photocatalytic activity.

The plots of  $(\alpha h\nu)^{1/2}$  versus energy for Ag<sub>3</sub>PO<sub>4</sub> and ABAP-48% are shown in Fig. 4(b). The  $E_{VB}$  and  $E_{CB}$  of Ag<sub>3</sub>PO<sub>4</sub> and AgBr can be respectively calculated according to the experiential formula (2) and (3) listed below:

$$E_{VB} = X - E_0 + 1/2E_g \quad (2)$$

$$E_{CB} = X - E_0 - 1/2E_g \quad (3)$$

where  $X$  is the absolute electronegativity of the semiconductor, and  $E_{VB}$  and  $E_{CB}$  are the potential of VB and CB, respectively. The value of  $E_0$  is 4.5 eV and  $E_g$  is the band gap energy of the semiconductor. The  $X$  values of AgBr and Ag<sub>3</sub>PO<sub>4</sub> are 5.81 eV and 5.96 eV, respectively. According to the UV-Vis DRS, the reckoned band gap energies of the as-synthesized pure Ag<sub>3</sub>PO<sub>4</sub> and AgBr were detected to be 2.42 and 2.50 eV, respectively. Based on the above experimental formula, the highest part of the VB and the lowest part of the CB of Ag<sub>3</sub>PO<sub>4</sub> are 2.67 eV and 0.25 eV, respectively. Simultaneously, the VB and CB of AgBr are detected to be 2.55 eV and 0.07 eV, respectively. In conclusion, the results of XRD, SEM and UV-Vis diffuse spectra proved the formation of the Ag<sub>3</sub>PO<sub>4</sub> heterojunction in ABAP nanoparticles, which may demonstrate high photocatalytic efficiency.

### 3.2 Photocatalytic performance

The photocatalytic activities of pure Ag<sub>3</sub>PO<sub>4</sub>, pure AgBr and ABAP composites were determined by the degradation of RhB

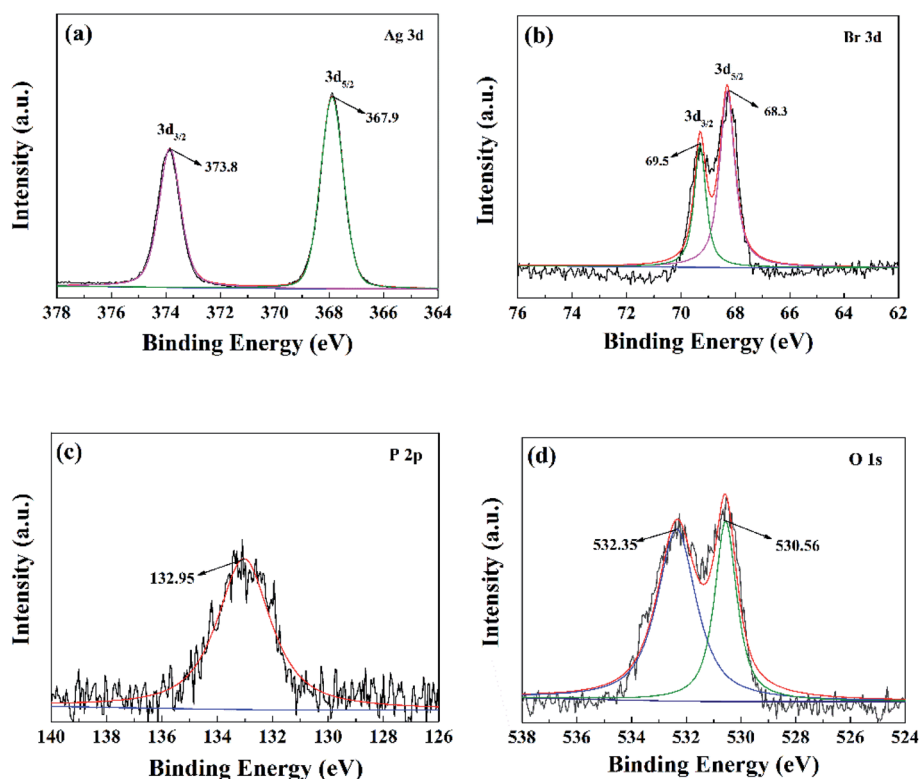


Fig. 3 XPS spectra of (a) Ag 3d, (b) Br 3d, (c) P 2p and (d) O 1s of the ABAP-48% composites.

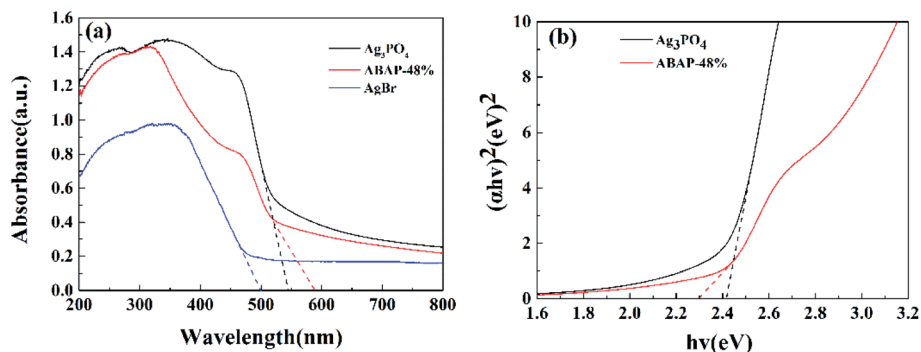


Fig. 4 UV-Vis diffuse reflectance spectra of (a):  $\text{Ag}_3\text{PO}_4$ ,  $\text{AgBr}$ ,  $\text{ABAP-48\%}$ ; (b) shows plot of  $(\alpha h\nu)^2$  versus energy ( $h\nu$ )  $\text{Ag}_3\text{PO}_4$  for and  $\text{ABAP-48\%}$ .

under visible light irradiation. The reusability tests were different from the original photocatalytic tests (Fig. 5); it was not necessary to detect every sample with a 5 min interval, only to compare the results after 25 min. After each test, the used sample was centrifuged and washed with deionized water three times, and dried for the next recycled photoactivity test. Before the light irradiation, the adsorption capability was primarily assessed in the absence of light. A liquid mixture of RhB and the resulting samples was vigorously stirred without irradiation for 0.5 h to achieve the adsorption-desorption equilibrium. It is shown in Fig. 5(a) that the concentration of RhB has only a minor decline without photocatalyst or without visible light irradiation, which indicated that the blank degradation was inappreciable. Under visible light illumination for 25 min,

about 62.1% and 69.1% of original RhB was eliminated by pure  $\text{Ag}_3\text{PO}_4$  and pure  $\text{AgBr}$ , respectively. It is obviously observed that the photocatalytic degradation capabilities of RhB are approximately 88.5%, 91.7%, 96.9%, 94.8% and 92.7% for  $\text{ABAP-16\%}$ ,  $\text{ABAP-32\%}$ ,  $\text{ABAP-48\%}$ ,  $\text{ABAP-64\%}$ ,  $\text{ABAP-80\%}$ , respectively, in the presence of visible light irradiation ( $\lambda > 400$ ) for 25 min. The  $\text{ABAP-48\%}$  sample displayed a much higher performance than the other different constant  $\text{ABAP-X\%}$  composites. However, at a higher theoretical molar ratio of Br relative to P ( $>48\%$ ), the photocatalytic activity decreased, indicating that a few active sites were covered with cohered  $\text{AgBr}$  coated on the surface of  $\text{Ag}_3\text{PO}_4$ . It suggested that the photocatalytic activities of the samples depended on the mass ratio of Br relative to P, demonstrating that  $\text{AgBr}$  played an important role in the

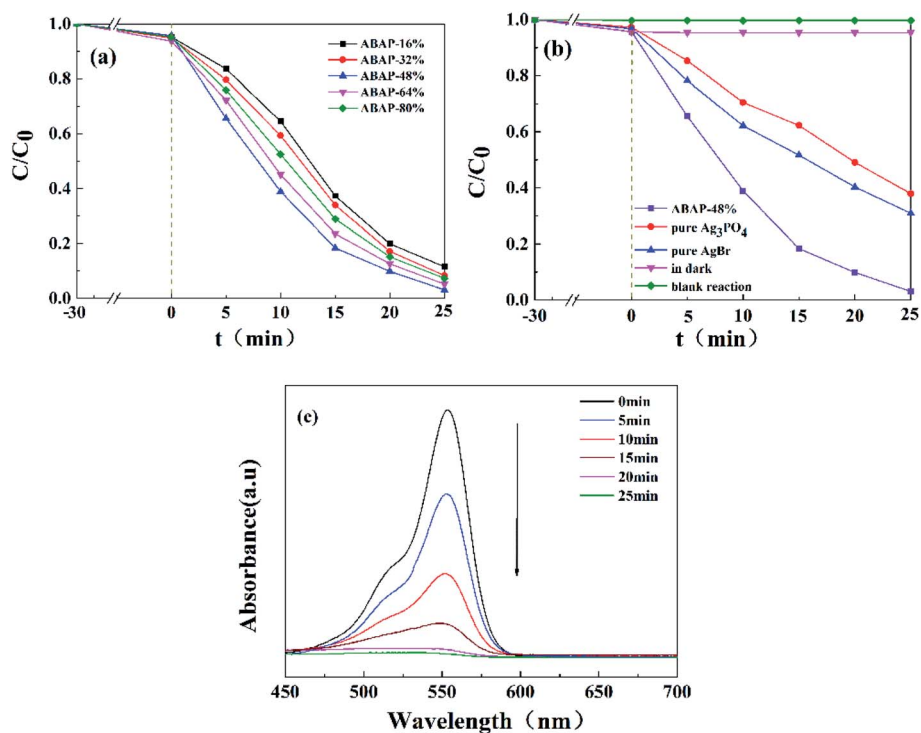


Fig. 5 (a) Photocatalytic activities of  $\text{ABAP-X\%}$  for RhB degradation under visible-light ( $\lambda > 420$  nm); (b) photocatalytic activities of numerous photocatalysts under visible-light ( $\lambda > 420$  nm); (c) UV-Vis spectral absorption changes of RhB solution photodegraded over the  $\text{ABAP-48\%}$  composite under visible light irradiation.

synergic effects between AgBr and Ag<sub>3</sub>PO<sub>4</sub>. As shown in Fig. 5(b), the intensity of the absorption spectra of RhB decreased by the ABAP-48% composite in the process of photocatalytic degradation. As the illumination time prolonged, the absorption peak intensity of RhB decreased step by step, and almost 100% of RhB degraded after illumination for 25 min.

To further investigate the major role of ABAP composites in the photocatalytic activity, a series of radical-trapping experiments were conducted by adding different scavengers. In general, several reactive intermediate species, such as h<sup>+</sup>, ·OH, and ·O<sub>2</sub><sup>-</sup>, are produced during the photocatalytic process. Hence, we used IPA, AO and BQ as the active scavengers for ·OH, h<sup>+</sup> and ·O<sub>2</sub><sup>-</sup>, respectively. As shown in Fig. 6, it can be observed that only a minor change was caused when IPA and AO were added to the reaction system for the photocatalytic degradation of RhB in the presence of ABAP-48% under visible light irradiation, which suggested that ·OH and h<sup>+</sup> were not the crucial active species in this reaction system. Conversely, when BQ was added, the photocatalytic activity was greatly suppressed, and the photo-degradation rate dropped to 25% compared to the no scavenger reaction under the same conditions, which indicated that ·O<sub>2</sub><sup>-</sup> played the main role in the reaction process (Fig. 7).

### 3.3 The possible mechanism of photocatalytic degradation

It is known that the efficient separation and transfer of photo-induced carriers at the heterojunction interfaces is an important strategy to improve the photocatalytic activity of composite photocatalysts.<sup>28</sup> Based on the above-mentioned results, a feasible photocatalytic mechanism of the as-synthesized ABAP composite under visible light irradiation is illustrated in Fig. 8. In this photocatalyst system, due to the irradiation of visible light, AgBr nanoparticles deposited on the surface of Ag<sub>3</sub>PO<sub>4</sub> nanoparticles can successfully reduce the solubility of Ag<sub>3</sub>PO<sub>4</sub> in the aqueous solution since AgBr nanoparticles can transfer or store electrons. Under visible light irradiation, both Ag<sub>3</sub>PO<sub>4</sub> and AgBr are induced as well as the photo-generated electron and hole pairs are distributed in their CB and VB, respectively. However, the band edge potential position of the Ag<sub>3</sub>PO<sub>4</sub> and

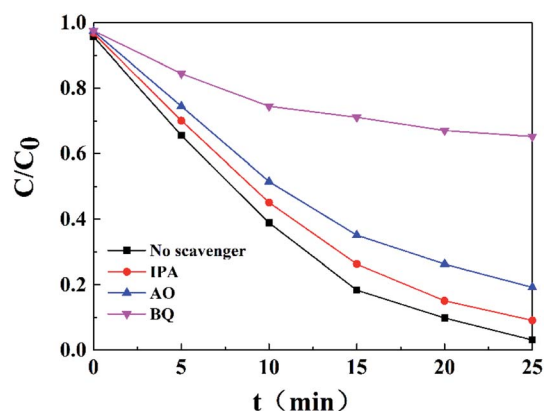


Fig. 6 Effects of different scavengers on the degradation of RhB over ABAP-48% under visible light irradiation.

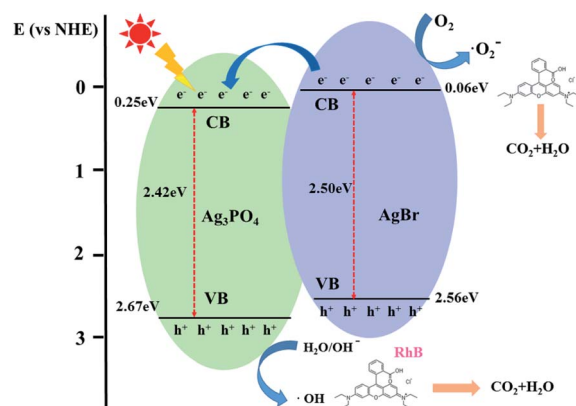


Fig. 7 Schematic showing the energy band structure and electron-hole pair separation in the ABAP-48% heterostructure under visible light irradiation.

ABAP composites had a significant influence on researching the process of photo-generated electron and hole pairs in the heterojunction. This made it difficult for the adsorbed water to be converted into ·OH radicals by light-induced holes. For the ABAP heterojunction photocatalysts, the CB and VB potentials of AgBr are more negative than those of the pristine Ag<sub>3</sub>PO<sub>4</sub>. The above-mentioned result shows that photo-induced electrons in AgBr immediately transferred to the CB of the Ag<sub>3</sub>PO<sub>4</sub> particles. The reaction of photo-induced electrons on the CB of Ag<sub>3</sub>PO<sub>4</sub> with molecular oxygen could produce superoxide radicals (·O<sub>2</sub><sup>-</sup>), which could engage in the photocatalytic decomposition process of RhB. It promoted the effective separation of photo-excited electron-hole pairs, and decreased the probability of electron-hole recombination, so RhB could be degraded more efficiently after the addition of AgBr. It suggested that the assembling of Ag<sub>3</sub>PO<sub>4</sub> and AgBr is beneficial to enhance the transfer of photo-generated electrons-hole pairs, decreasing the possibility of the recombination of photo-excited carriers, and accelerating the generation of more ·O<sub>2</sub><sup>-</sup>. Thus, the photocatalytic activity of pristine particles could be tremendously enhanced after the addition of AgBr.

### 3.4 The recyclability study

In addition to the photocatalytic activity, another significant factors for the practical application of composite photocatalysts are stability and reusability. Under visible light irradiation, the as-prepared ABAP composites were also investigated by the circulating runs in the photocatalytic degradation of RhB to evaluate the stability. As shown in Fig. 8(a), the photocatalytic performance of pure Ag<sub>3</sub>PO<sub>4</sub> showed a notable loss after five cycles, while that of the ABAP-48% composite remained at 82%, which indicated that the AgBr nanoparticles anchoring on the surface of Ag<sub>3</sub>PO<sub>4</sub> nanoparticles can obviously decrease the solubility of Ag<sub>3</sub>PO<sub>4</sub> in the aqueous solution. Thus, the structural stability of ABAP composites considerably increased in the photocatalytic processes. The crystalline structures of the ABAP-48% nanocomposite were investigated before and after reactions to assess the structural stability. Fig. 8(b) displays the XRD

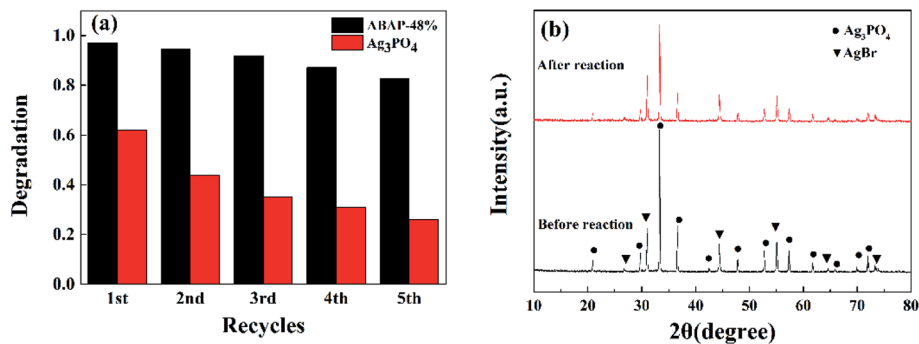


Fig. 8 (a) The cycling runs in the photocatalytic degradation of RhB over ABAP-48% and pure  $\text{Ag}_3\text{PO}_4$  under visible light irradiation; (b) XRD patterns of ABAP-48% after the photocatalytic reaction.

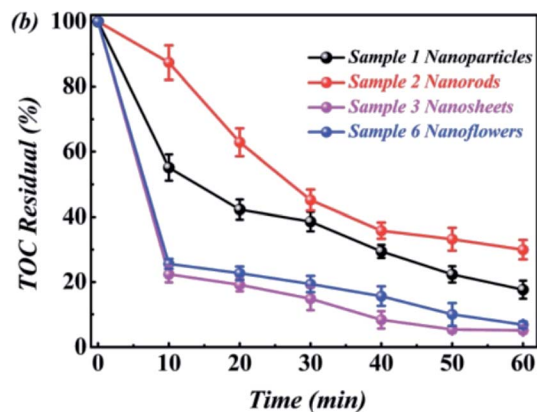


Fig. 9 The TOC removal of RhB degradation products.

patterns of ABAP-48% before and after circulating experiments. No distinct structure or integrity changes of the photocatalyst can be observed in the XRD pattern, which indicates that AgBr enhances the stability of the  $\text{Ag}_3\text{PO}_4$  photocatalyst. In short, a certain amount of AgBr attached to the surface of the  $\text{Ag}_3\text{PO}_4$  nanoparticles can evidently enhance the photocatalytic activity and stability of the ABAP composites compared to the original  $\text{Ag}_3\text{PO}_4$ . This result shows that the composites can be widely used in the photocatalytic degradation of numerous organic pollutants in waste water as a series of hopeful photocatalysts.

### 3.5 Determination of TOC after waste liquid degradation

The total organic carbon (TOC) analysis of the RhB solution was carried out using a WTW's photoLab S12 analyzer. Taking sample ABAP-48% as an example, Fig. 9 shows the TOC removal of RhB degradation products. About 99% of TOC was removed within 40 min in the presence of ABAP-48%, demonstrating that RhB was oxidized by oxidative radicals to  $\text{CO}_2$ ,  $\text{H}_2\text{O}$ , and  $\text{NO}_3^-$ , indicating that the photocatalytic RhB oxidation process did not produce secondary harmful species.

## 4. Conclusion

In summary, in this study, different contents of AgBr nanoparticles deposited on  $\text{Ag}_3\text{PO}_4$  polyhedral structure particles

were successfully prepared by the anion-exchange of  $\text{Br}^-$  with  $\text{PO}_4^{3-}$ . AgBr nanoparticles with sizes of less than 7 nm were evenly anchored on the surface of  $\text{Ag}_3\text{PO}_4$  polyhedral structure particles. The ABAP-48% composites exhibited a much higher activity than original  $\text{Ag}_3\text{PO}_4$  and AgBr for the decomposition of RhB, which simulated dyes in waste water. This could be profited from the stronger response to visible light and photo-induced electron and hole separation and transfer mechanism. It is suggested that  $\text{O}_2^-$  played an important role in the photocatalytic degradation of RhB by ABAP composite photocatalysts in the presence of visible light. Moreover, the ABAP-48% composites showed an excellent photocatalytic activity after five recycling runs, which demonstrated the high stability. Consequently, ABAP composites synthesized by the one pot method had obvious advantages in the waste water treatment and environmental restoration under an irradiation with visible light.

## Conflicts of interest

We declare that we have no financial and personal relationships with other people or organizations that can inappropriately influence our work; there is no professional or other personal interest of any nature or kind in any product, service and/or company that could be construed as influencing the position presented in, or the review of, the manuscript entitled, "One-pot synthesis of AgBr/ $\text{Ag}_3\text{PO}_4$  composite photocatalyst for enhancing visible photocatalytic degradation of RhB".

## Acknowledgements

This research was financially supported to both the Industrialization project of the 13th Five-year Plan of Jilin provincial Department of Education of China (no. JJKH20200683KJ) and the Environmental Protection Research Project of Ecology and Environment Department of Jilin Province of China (no. 202006).

## References

- 1 J. Ma, C. Chen and F. Yu, Self-regenerative and self-enhanced smart graphene/ $\text{Ag}_3\text{PO}_4$  hydrogel adsorbent under visible light, *New J. Chem.*, 2016, **40**, 3208–3215.

- 2 N. M. Mahmoodi, Surface modification of magnetic nanoparticle and dye removal from ternary systems, *J. Ind. Eng. Chem.*, 2015, **27**, 251–259.
- 3 K. Singh and S. Arora, Removal of synthetic textile dyes from wastewaters: a critical review on present treatment technologies, *Crit. Rev. Environ. Sci. Technol.*, 2011, **41**, 807–878.
- 4 X. Yu, L. Gao, J. Huang, W. Li, G. B. Liu, Z. H. Lia, J. W. Liu and P. A. Hu, Construction of hybrid  $\text{Ag}_2\text{CO}_3/\text{AgVO}_3$  nanowires with enhanced visible light photocatalytic activity, *Mater. Res. Bull.*, 2018, **101**, 246–252.
- 5 C. S. Zhu, L. Zhang, B. Jiang, J. T. Zheng, P. Hu, S. J. Li, M. B. Wu and W. T. Wu, Fabrication of Z-scheme  $\text{Ag}_3\text{PO}_4/\text{MoS}_2$  composites with enhanced photocatalytic activity and stability for organic pollutant degradation, *Appl. Surf. Sci.*, 2016, **377**, 99–108.
- 6 D. J. Martin, G. G. Liu, S. J. A. Moniz, Y. P. Bi, A. M. Beale, J. H. Ye and J. W. Tang, Cheminform abstract: efficient visible driven photocatalyst, silver phosphate: performance, understanding and perspective, *Chem. Soc. Rev.*, 2015, **44**, 7808–7828.
- 7 T. J. Yan, H. W. Zhang, Y. P. Liu and J. M. You, Fabrication of robust  $\text{M}/\text{Ag}_3\text{PO}_4$  ( $\text{M} = \text{Pt}, \text{Pd}, \text{Au}$ ) Schottky-type heterostructures for improved visible-light photocatalysis, *RSC Adv.*, 2014, **4**, 37220–37230.
- 8 C. Jin, G. L. Liu, L. H. Zu, Y. Qin and J. H. Yang, Preparation of  $\text{Ag}@\text{Ag}_3\text{PO}_4/\text{ZnO}$  ternary heterostructures for photocatalytic studies, *J. Colloid Interface Sci.*, 2015, **453**, 36–41.
- 9 W. R. Cao, Y. T. An, L. F. Chen and Z. W. Qi, Visible-light-driven  $\text{Ag}_2\text{MoO}_4/\text{Ag}_3\text{PO}_4$  composites with enhanced photocatalytic activity, *J. Alloys Compd.*, 2017, **701**, 350–357.
- 10 J. Tian, T. J. Yan, Z. Qiao, L. L. Wang, W. J. Li, J. M. You and B. B. Huang, Anion-exchange synthesis of  $\text{Ag}_2\text{S}/\text{Ag}_3\text{PO}_4$  core/shell composites with enhanced visible and NIR light photocatalytic performance and the photocatalytic mechanisms, *Appl. Catal., B*, 2017, **209**, 566–578.
- 11 Q. Li, F. Wang, Y. Hua, Y. Luo, G. Duan and X. Yang, Deposition-precipitation preparation of  $\text{Ag}/\text{Ag}_3\text{PO}_4/\text{WO}_3$  nanocomposites for efficient Visible-light degradation of rhodamine B under strongly acidic/alkaline conditions, *J. Colloid Interface Sci.*, 2017, **506**, 207–216.
- 12 L. Li, Y. H. Qi, J. R. Lu, S. L. Lin, W. J. An, Y. H. Liang and W. Q. Cui, A stable  $\text{Ag}_3\text{PO}_4/\text{g-C}_3\text{N}_4$  hybrid core@shell composite with enhanced visible light photocatalytic degradation, *Appl. Catal., B*, 2016, **183**, 133–141.
- 13 H. R. Wang, L. Zou, Y. C. Shan and X. Wang, Ternary  $\text{GO}/\text{Ag}_3\text{PO}_4/\text{AgBr}$  composite as an efficient visible-light-driven photocatalyst, *Mater. Res. Bull.*, 2017, **97**, 189–194.
- 14 Q. Y. Chen, Y. F. Wang, Y. W. Wang, X. C. Zhang, D. H. Duan and C. M. Fan, Nitrogen-doped carbon quantum dots/ $\text{Ag}_3\text{PO}_4$  complex photocatalysts with enhanced visible light driven photocatalytic activity and stability, *J. Colloid Interface Sci.*, 2017, **491**, 238–245.
- 15 S. S. Yao, S. K. Xue, J. H. Zhang and X. Q. Shen, Characterization and mechanism analysis of AgBr mixed cuboid  $\text{WO}_3$  rods with enhanced photocatalytic activity, *RSC Adv.*, 2016, **6**(96), 93436–93444.
- 16 D. J. Wang, L. Guo, Y. Z. Zhen and L. L. Yue, AgBr quantum dots decorated mesoporous  $\text{Bi}_2\text{WO}_6$  architectures with enhanced photocatalytic activities for methylene blue, *J. Mater. Chem. A*, 2014, **2**, 11716–11727.
- 17 P. Amornpitoksuk and S. Suwanboon, Photocatalytic degradation of dyes by  $\text{AgBr}/\text{Ag}_3\text{PO}_4$ , and the ecotoxicities of their degraded products, *Chin. J. Catal.*, 2016, **37**, 711–719.
- 18 A. A. Abdel-Khalek, S. A. Mahmoud and A. H. Zaki, Visible light assisted photo-catalytic degradation of Crystal Violet, Bromophenol Blue and Eosin Y dyes using  $\text{AgBr-ZnO}$  nanocomposite, *Environ. Nanotechnol. Monit. Manage.*, 2018, **9**, 164–173.
- 19 L. S. Zhong, C. H. Hu, J. Zhuang, Y. Zhong, D. H. Wang and H. Y. Zhou,  $\text{AgBr}/\text{MgBi}_2\text{O}_6$  heterostructured composites with highly efficient visible-light-driven photocatalytic activity, *J. Phys. Chem. Solids*, 2018, **117**, 94–100.
- 20 J. H. Qu, X. Wang, Y. G. Zhang and G. L. Yuan, Multifunctional Ag nanoparticles in heterostructured  $\text{Ag}_2\text{MoO}_4/\text{Ag}/\text{AgBr}$  cubes with boosted photocatalytic performances, *Sol. Energy*, 2018, **170**, 124–131.
- 21 X. L. Miao, X. P. Shen, J. J. Wu, Z. Y. Ji, J. H. Wang, L. R. Kong, M. M. Liu and C. S. Song, Fabrication of an all solid Z-scheme photocatalyst  $\text{g-C}_3\text{N}_4/\text{GO}/\text{AgBr}$  with enhanced visible light photocatalytic activity, *Appl. Catal., B*, 2017, **539**, 104–113.
- 22 B. Wang, X. Q. Gu, Y. L. Zhao and Y. H. Qiang, A comparable study on the photocatalytic activities of  $\text{Ag}_3\text{PO}_4$ , AgBr and  $\text{AgBr}/\text{Ag}_3\text{PO}_4$  hybrid microstructures, *Appl. Surf. Sci.*, 2013, **283**, 396–401.
- 23 J. R. Chen, X. Y. Yang, C. Y. Zhu, X. Xin, C. P. Lin, Y. L. Zhao and Q. S. Yan, A research on shape-controllable synthesis of  $\text{Ag}_3\text{PO}_4/\text{AgBr}$  and its degradation of ciprofloxacin, *Water Sci. Technol.*, 2018, **77**, 1230–1237.
- 24 Y. G. Kim and W. K. Jo, Efficient decontamination of textile industry waste water using a photochemically stable n-n type  $\text{CdSe}/\text{Ag}_3\text{PO}_4$  heterostructured nanohybrid containing metallic Ag as a mediator, *J. Hazard. Mater.*, 2019, **361**, 64–72.
- 25 L. J. Di, H. Yang, T. Xian and X. J. Chen, Facile Synthesis and enhanced visible-light photocatalytic activity of novel p- $\text{Ag}_3\text{PO}_4/\text{n-BiFeO}_3$  heterojunction composites for dye degradation, *Nanoscale Res. Lett.*, 2018, **13**, 257–269.
- 26 Y. Hu, J. J. Li, Y. L. Xie and Y. J. Zhong, Facile synthesis of Z-scheme  $\text{Ag}_2\text{CO}_3/\text{Ag}/\text{AgBr}$  ternary heterostructured nanorods with improved photostability and photoactivity, *J. Mater. Chem. A*, 2015, **3**, 5474–5481.
- 27 Q. S. Dong, Z. B. Jiao, H. C. Yu and J. H. Ye, Facile synthesis of hollow  $\text{Ag}@\text{AgBr}$  heterostructures with highly efficient visible-light photocatalytic properties, *Crystengcomm*, 2014, **16**, 8317–8321.
- 28 X. Li, T. Wan, J. Qiu, H. Wei, F. Qin, Y. Wang, Y. Liao, Z. Huang and X. Tan, In-situ photocalorimetry-fluorescence spectroscopy studies of RhB photocatalysis over Z scheme  $\text{g-C}_3\text{N}_4/\text{Ag}@\text{Ag}_3\text{PO}_4$  nanocomposites:



- a pseudo-zero-order rather than a first-order process, *Appl. Catal., B*, 2017, **217**, 591–602.
- 29 H. Katsumata, T. Sakai, T. Suzuki and S. Kaneco, Highly efficient photocatalytic activity of *g*-C<sub>3</sub>N<sub>4</sub>/Ag<sub>3</sub>PO<sub>4</sub> hybrid photocatalysts through Z-scheme photocatalytic mechanism under visible light, *Ind. Eng. Chem. Res.*, 2014, **53**, 8018–8025.
- 30 R. K. Chava, J. Y. Do and M. Kang, Fabrication of CdS-Ag<sub>3</sub>PO<sub>4</sub> heteronanostructures for improved visible photocatalytic hydrogen evolution, *J. Alloys Compd.*, 2017, **727**, 86–93.
- 31 Y. Bu, Z. Chen and C. Sun, Highly efficient Z-Scheme Ag<sub>3</sub>PO<sub>4</sub>/Ag/WO<sub>3-x</sub> photo-catalyst for its enhanced photocatalytic performance, *Appl. Catal., B*, 2015, **179**, 363–371.
- 32 W. R. Cao, Y. T. An, L. F. Chen and Z. W. Qi, Visible-light-driven Ag<sub>2</sub>MoO<sub>4</sub>/Ag<sub>3</sub>PO<sub>4</sub>, composites with enhanced photocatalytic activity, *J. Alloys Compd.*, 2017, **701**, 350–357.